Report

Neuron

Binary Fate Choice between Closely Related Interneuronal Types Is Determined by a Fezf1-Dependent Postmitotic Transcriptional Switch

Graphical Abstract

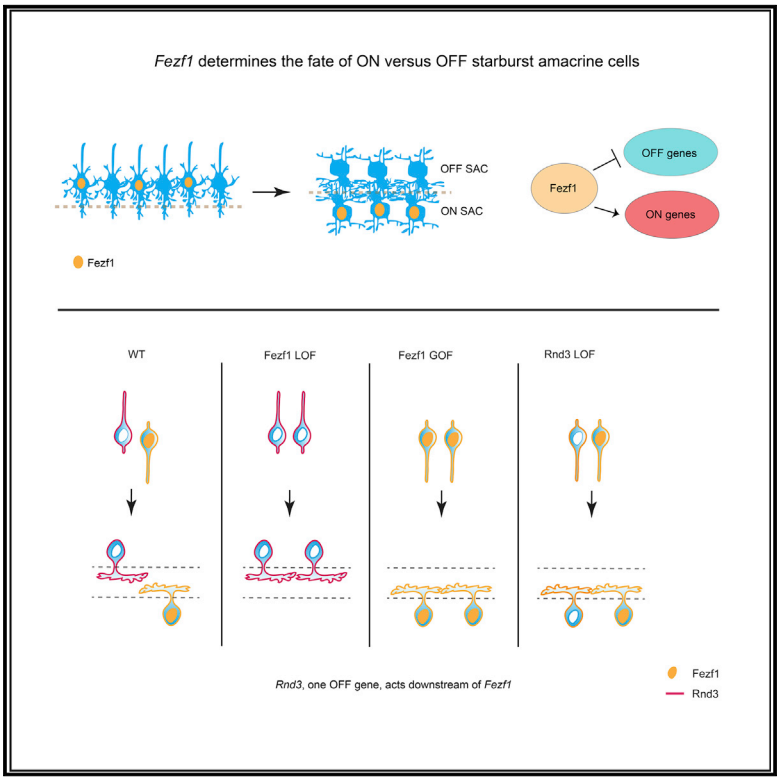

Highlights

- ON and OFF SACs are transcriptionally distinct prior to migration
- Fezf1 is selectively expressed by newly postmitotic ON SACs
- Fezf1 functions as a fate switch by activating ON and repressing OFF SAC genes
- Rnd3 acts downstream of Fezf1 to enable distinct positioning of ON and OFF SACs

Authors

Yi-Rong Peng, Rebecca E. James, Wenjun Yan, Jeremy N. Kay, Alex L. Kolodkin, Joshua R. Sanes

Correspondence

kolodkin@jhmi.edu (A.L.K.), sanesj@mcb.harvard.edu (J.R.S.)

In Brief

Two related retinal cell types called ON and OFF starburst amacrines migrate to distinct laminae and signal increased (ON) or decreased (OFF) illumination. Fezf1 acts as a fate switch between the two types by activating ON and repressing OFF genes.

Peng et al., 2020, Neuron *105*, 1–11
February 5, 2020
https://doi.org/10.1016/j.neuron.2019.11.002

CellPress

Please cite this article in press as: Peng et al., Binary Fate Choice between Closely Related Interneuronal Types Is Determined by a Fezf1-Dependent Postmitotic Transcriptional Switch, Neuron (2019), https://doi.org/10.1016/j.neuron.2019.11.002

Neuron
Report

Binary Fate Choice between Closely Related Interneuronal Types Is Determined by a Fezf1-Dependent Postmitotic Transcriptional Switch

Yi-Rong Peng,[1,4] Rebecca E. James,[2,4] Wenjun Yan,[1] Jeremy N. Kay,[3] Alex L. Kolodkin,[2,*] and Joshua R. Sanes[1,5,*]
[1]Center for Brain Science and Department of Molecular and Cellular Biology, Harvard University, Cambridge, MA 02138, USA
[2]Solomon H. Snyder Department of Neuroscience, The Johns Hopkins University School of Medicine, Baltimore, MD 21205, USA
[3]Departments of Ophthalmology and Neurobiology, Duke University Medical Center, Durham, NC, USA
[4]These authors contributed equally
[5]Lead Contact
*Correspondence: kolodkin@jhmi.edu (A.L.K.), sanesj@mcb.harvard.edu (J.R.S.)
https://doi.org/10.1016/j.neuron.2019.11.002

SUMMARY

Many neuronal types occur as pairs that are similar in most respects but differ in a key feature. In some pairs of retinal neurons, called paramorphic, one member responds to increases and the other to decreases in luminance (ON and OFF responses). Here, we focused on one such pair, starburst amacrine cells (SACs), to explore how closely related neuronal types diversify. We find that ON and OFF SACs are transcriptionally distinct prior to their segregation, dendritic outgrowth, and synapse formation. The transcriptional repressor Fezf1 is selectively expressed by postmitotic ON SACs and promotes the ON fate and gene expression program while repressing the OFF fate and program. The atypical Rho GTPase Rnd3 is selectively expressed by OFF SACs and regulates their migration but is repressed by Fezf1 in ON SACs, enabling differential positioning of the two types. These results define a transcriptional program that controls diversification of a paramorphic pair.

INTRODUCTION

In many parts of the nervous system, one finds pairs of neuronal types that are similar in most respects but differ in a key feature. For example, select pairs of similar mammalian geniculocortical neuron types project to the visual cortex and differ primarily in their response properties to changes in luminance (Usrey and Fitzpatrick, 1996). Many such pairs are present in the retina, some of which have been called "paramorphic," with one member responding to increases (ON cells) and the other to decreases (OFF cells) in light intensity (Famiglietti, 2004, 2005; Rousso et al., 2016). Because inputs that endow retinal neurons with ON and OFF responses are segregated to the inner and outer portions of a synaptic region called the inner plexiform layer (IPL), the key structural difference between members of these pairs is the position of their dendrites within the IPL (Figure 1A).

In few, if any, cases do we know when, where, or how these closely related types acquire their distinct characteristics. To address these issues, we focus here on a paramorphic pair of retinal interneurons called starburst amacrine cells (SACs). SACs are cholinergic retinal interneurons that are critical for computing the direction of moving objects (Vaney et al., 2012). As is the case for other paramorphic pairs, ON and OFF SACs have dendrites in the ON and OFF sublaminae of the IPL, respectively; in addition, their somata are differentially positioned, with ON SACs in the ganglion cell layer (GCL) and OFF SACs in the inner nuclear layer (INL) (Figure 1A). SACs are so closely anatomically and functionally related that they have been considered mirror-symmetric cells, differing only with respect to soma and dendritic arbor placement (Famiglietti, 1983; Vaney et al., 2012).

Using single cell transcriptomic profiling, we establish that ON and OFF SACs are transcriptionally distinct cell types, not mirror-symmetric versions of a single type. We show that differential gene expression patterns arise during SAC migration and identify the transcriptional regulator *Fezf1* as a critical determinant of the ON phenotype. Fezf1 acts postmitotically to specify the ON and repress the OFF SAC fates, in part by regulating the atypical Rho GTPase *Rnd3*/*RhoE* (hereafter *Rnd3*) to promote distinct SAC migratory programs. These results identify a gene expression program that diversifies ON and OFF SACs shortly after they become postmitotic but before they complete migration, thereby determining their somatic and dendritic positions without affecting the many properties they share.

RESULTS

ON and OFF Starburst Amacrine Cells Are Transcriptomically Distinct

SACs in the central mouse retina are born at the apical edge of the retinal neuroblast layer (NBL) from around embryonic day (E) 10 to E14 (Voinescu et al., 2009). They then migrate basally to reach the border of the outer and inner neuroblast layers (ONBL, INBL). After E16, about half continue basally to the INBL, where they become ON SACs; the others remain in the

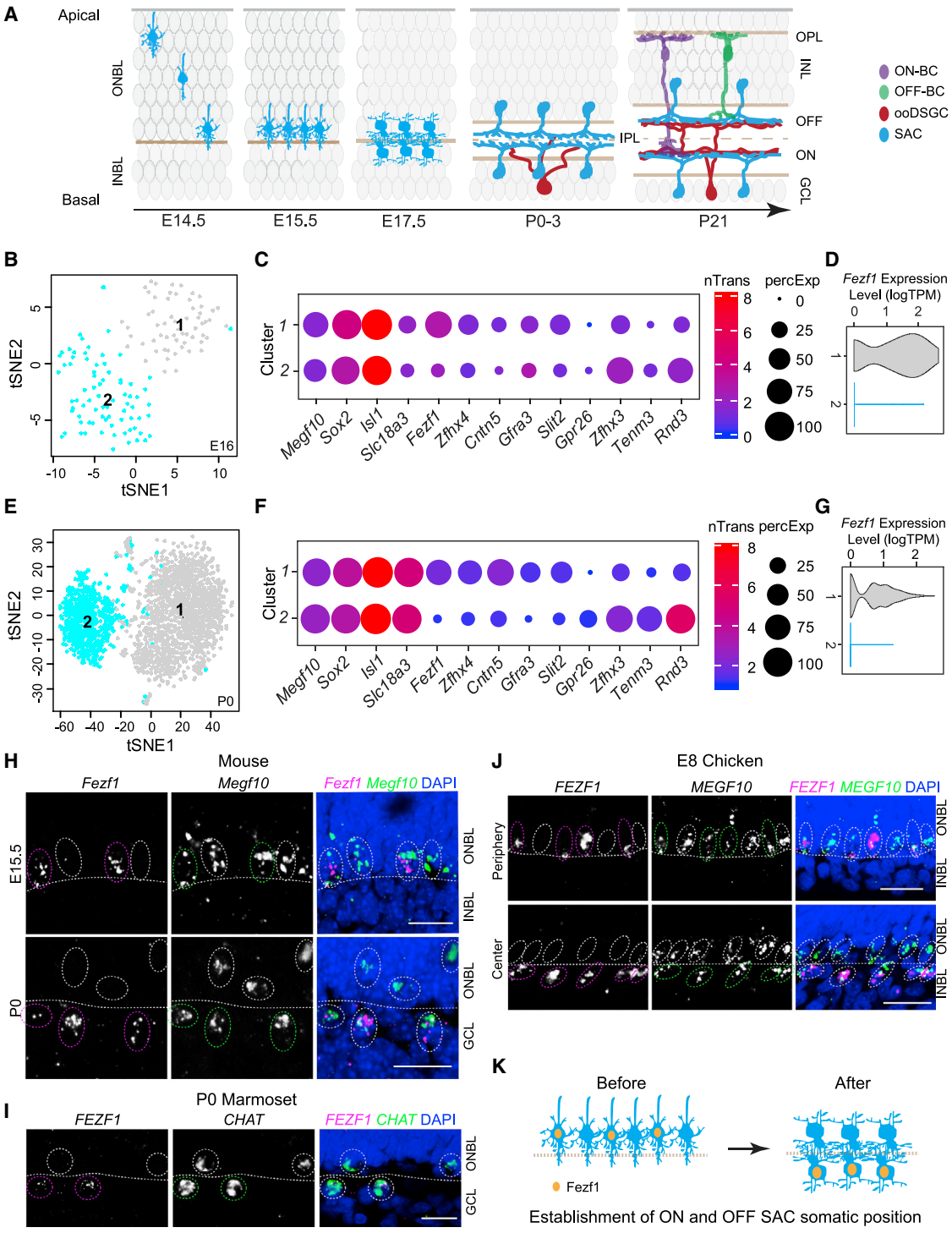

Figure 1. ON and OFF Starburst Amacrine Cells Are Transcriptionally Distinct Subtypes Distinguished by *Fezf1*

(A) Development of SACs. BC, bipolar cell; GCL, ganglion cell layer; INBL, inner neuroblastic layer; INL, inner nuclear layer; IPL, inner plexiform layer; ONBL, outer neuroblastic layer; ooDSGC, ON-OFF direction-selective ganglion cell; OPL, outer plexiform layer.

(B) t-Distributed stochastic neighbor embedding (tSNE) visualization of 136 SACs sequenced at E16.

(C) Dot plot of select genes expressed by clusters 1 and 2 of the E16 SAC dataset. *Megf10*, *Sox2*, *Isl1*, and *Slc18a3* are known SAC marker genes (left). Genes of interest are largely selected from the P0 differentially expressed (DE) gene list. DE genes that achieve statistical significance at E16 as defined in STAR Methods are *Fezf1*, *Zfhx3*, and *Rnd3*.

(D) Violin plot of *Fezf1* expression in the two E16 SAC clusters.

(legend continued on next page)

ONBL and become OFF SACs (Figure S1C; Knabe et al., 2007; Thangaraj et al., 2012). Over the next few days the ONBL and INBL become the INL and GCL, respectively, the border between them becomes the IPL, and SACs extend dendrites into the IPL (Ray et al., 2018; Stacy and Wong, 2003). During the first postnatal week, ON and OFF bipolar cells begin making synapses onto SACs, and the SACs begin making synapses onto retinal ganglion cells (RGCs). SACs are fully integrated into direction-selective circuits by the time of eye opening at postnatal day (P) 14 (Figure 1A).

When we began our studies, few molecular differences between ON and OFF SACs were known. Purinergic receptor P2x (*P2rx2*) was detected in OFF but not ON SACs (Kaneda et al., 2010), and glycine receptor subunit alpha 4 (*Glra4*) was detected in ON but not OFF SACs (Heinze et al., 2007), but these differences were apparent only in mature retina. To ask whether differences arise before SACs reach their final positions, we performed single-cell RNA sequencing (scRNA-seq) on 136 SACs at E16 (Figures 1B–1D and S1A; see STAR Methods) and 2,055 SACs at P0, after migration is complete but before synapses form (Figures 1E–1G). All of the sequenced cells were enriched for genes expressed by ON and OFF SACs (including *Megf10*, *Sox2*, *Isl1*, and *Slc18a3*, which encodes the vesicular acetylcholine transporter [VAChT]). Markers of other retinal neuron types, including *Crx* (cones and rods), *Nrl* (rods), *Vsx2* (Chx10, bipolar cells), *Lhx1* (horizontal cells), *Pou4f1* (RGCs), and *Hes5* (progenitor cells), were expressed at very low levels, if at all (Figure S1B).

At both ages, we identified two distinct clusters of SACs that we suspected represented ON and OFF types. To test this idea, we used fluorescence *in situ* hybridization (FISH) to assess differentially expressed genes. *Fezf1*, *Gfra3*, and *Slit2*, which were enriched in cluster 1, were all selectively expressed in ON SACs, whereas *Tenm3* and *Rnd3* were enriched in cluster 2 and selectively expressed in OFF SACs (Figures 1C, 1F, 1H, and S1C; see below). Moreover, *Cntn5*, which we recently showed is an ON SAC marker (Peng et al., 2017), was enriched in cluster 1. Together these results show that clusters 1 and 2 comprise ON and OFF SACs, respectively, demonstrating that these neuronal types are transcriptionally distinct while their somata are still intermingled and before they extend dendrites or form synapses.

Fezf1 Is Expressed by Postmitotic ON Starburst Amacrine Cells

Fezf1 and its homolog Fezf2 have been implicated in the specification and differentiation of several central neuronal types, although roles of Fezf1 have been difficult to study because of redundancy with Fezf2 (Eckler and Chen, 2014). We were intrigued to note that *Fezf1* was selectively expressed by ON SACs and that *Fezf2* was not detectably expressed by either SAC type (Figure S1B). We therefore analyzed *Fezf1* expression in detail using FISH.

Fezf1 was undetectable at E13.5, but it was present in a sparse population of cells in the basal ONBL at E14.5 and E15.5 (Figures 1H and S1D). Double labeling with the pan-SAC marker *Megf10* (Kay et al., 2012) demonstrated that *Fezf1*-positive cells constituted a subset of SACs, presumably those destined to be ON SACs (Figure 1H). By E17.5, the *Fezf1*-positive SACs had migrated to the INBL (Figure S1E). Selective expression of *Fezf1* by ON but not OFF SACs was maintained after birth, although levels decreased during the second postnatal week (Figures S1E and S1F).

Fezf1 Expression by ON Starburst Amacrine Cells Is Evolutionarily Conserved

ON and OFF SACs are present in most, if not all, vertebrate species (Zhang et al., 2019). We asked whether *Fezf1* expression is a conserved feature of ON SACs by analyzing marmoset (*Callithrix jacchus*) and chicken (*Gallus gallus domesticus*) retinas. Double FISH of *FEZF1* and *CHAT* revealed select expression of *FEZF1* in ON SACs of the neonatal marmoset retina (Figure 1I). In chicks, we analyzed retinas at E8. At that stage, because of a central to peripheral developmental gradient, ON and OFF SACs have segregated into distinct cellular layers (INBL and ONBL) in the central retina but remain intermingled in the ONBL of the peripheral retina. As seen in mouse, *FEZF1* is selectively expressed by ON SACs in central retina at this time, but by only about half of the migratory SACs in peripheral retina (Figure 1J). Thus, *Fezf1* is selectively expressed by ON SACs in multiple vertebrate species and, at least in chick and mouse, is expressed by a subset of SACs prior to the completion of their migration.

Fezf1 Determines the Position of ON Starburst Amacrine Cells

To study Fezf1 during SAC development, we used a reporter line, $Fezf1^{GFP}$, in which GFP replaces the coding region of *Fezf1* to generate a null allele (Eckler et al., 2011; Figure S2A). Thus, GFP marks cells that express *Fezf1* in heterozygotes ($Fezf1^{GFP/+}$) and cells that were fated to express *Fezf1* in homozygotes ($Fezf1^{GFP/GFP}$). As expected from FISH results, GFP was expressed exclusively by a subset of SACs in $Fezf1^{GFP/+}$ retinas between E14.5 and P0 and by ON SACs postnatally (Figures 2A and S2B). A small percentage of GFP-positive SACs remained in the INL of P0 $Fezf1^{GFP/+}$ retinas (Figure 2C), suggesting that ON SAC migration is incomplete at birth. After P6, GFP was also expressed by the bipolar cell type BC1b (Figure S2C), consistent with our previous observations (Shekhar et al., 2016). The $Fezf1^{GFP}$ allele also allowed us to determine if *Fezf1* is expressed by SAC progenitors. The absence of the progenitor marker Ki67 in GFP cells indicated that detectable *Fezf1* expression is confined to postmitotic SACs (Figure S2D).

(E–G) Same as (B–D) for 2,055 SACs sequenced at P0.

(H–J) Double fluorescence *in situ* hybridization (FISH) using probes against *Fezf1* (magenta) and *Megf10* or *CHAT* (green) to label SACs in E15.5 and P0 mouse retina (H), P0 marmoset retina (I), and the peripheral (top) and central (bottom) regions of E8 chicken retina (J). Among *Megf10*- or *CHAT*-positive SACs, *Fezf1*-positive cells are ON SACs while negatives are OFF SACs. *FEZF1*- and *CHAT*-positive cells in marmoset are ON SACs.

(K) Model of *Fezf1*-expressing SAC soma position before and after ON and OFF SAC soma segregation.

Scale bars are 20 μm. SAC somata are outlined by circles, and white dashed lines indicate the ONBL and INBL border. See also Figure S1.

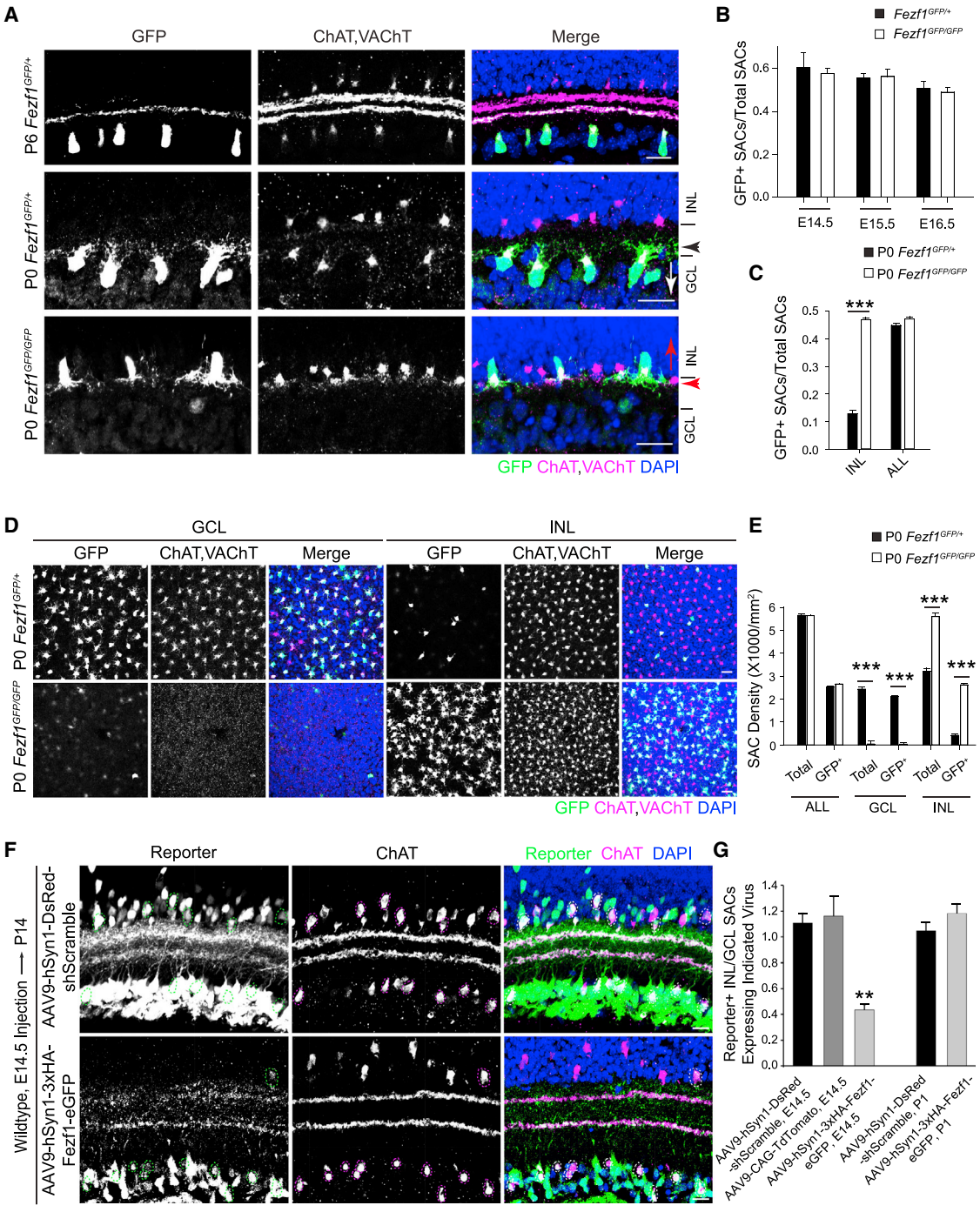

Figure 2. *Fezf1* Determines the Position of ON Starburst Amacrine Cells

(A) GFP-labeled ON SACs from P6 *Fezf1*$^{GFP/+}$ (top), P0 *Fezf1* $^{GFP/+}$ (middle), and P0 *Fezf1*$^{GFP/GFP}$ (bottom) retinas. All SACs are labeled with antibodies against ChAT and VAChT. ON SACs are GFP positive (green). In *Fezf1*$^{GFP/+}$ retinas (top and middle), ON SACs are localized in the GCL, while OFF SACs are localized in the INL. In *Fezf1*$^{GFP/GFP}$ retinas (bottom), GFP-positive SACs are in the INL alongside OFF SACs (GFP negative, ChAT/VAChT positive). White and red arrows mark the position and orientation of ON SACs; arrowheads mark the stratification levels of ON SAC dendrites within the IPL.

(B) Ratios of GFP-positive SACs to total SACs at indicated embryonic time points in *Fezf1* $^{GFP/+}$ and *Fezf1*$^{GFP/GFP}$ retinas. Example images are in Figure S2A. Bars show mean ± SEM from one to three sections from each of three or four animals.

(C) Ratios of GFP-positive SACs to total SACs observed either in the INL or in the INL and GCL (ALL) in *Fezf1*$^{GFP/+}$ or *Fezf1*$^{GFP/GFP}$ retinas. Bars show mean ± SEM from eight images from each of three or four animals. Example images are in (D).

(D) *En face* views of GFP-labeled SACs in the GCL (left) and INL (right) of *Fezf1* $^{GFP/+}$ (top) and *Fezf1*$^{GFP/GFP}$ (bottom) retinas.

(legend continued on next page)

To determine if *Fezf1* plays a role in ON SACs, we examined *Fezf1*$^{GFP/GFP}$ retinas. We detected no defects in overall retinal structure or development between E14.5 and ~P1–P2, when *Fezf1*$^{GFP/GFP}$ mice die (Eckler et al., 2011). A normal cohort of SACs was present in mutants as early as E14.5, and the fraction that was GFP positive was unaffected by *Fezf1* deletion (Figures 2B and S2B). Strikingly, ON SACs were almost entirely depleted from the GCL in *Fezf1* mutants and were instead found intermixed with OFF SACs (GFP negative, ChAT/VAChT positive) in the INL. This defect was apparent both in sectioned (Figure 2A) and whole-mount (Figure 2D) retinas. SAC density was decreased by >90% in the GCL and correspondingly increased in the INL, with no significant change in the overall number of SACs (ChAT/VAChT positive) or the fraction of SACs that were GFP positive (Figures 2C and 2E). Thus, Fezf1 has no detectable effect on the generation of SACs, but it is required for their translocation into the INBL.

To test if Fezf1 is sufficient to promote SAC migration into the INBL, we generated an adeno-associated viral (AAV) vector that expresses an epitope (3xHA)-tagged Fezf1 and GFP, driven by a human synapsin 1 promoter (hSyn1). We used AAV serotype 9, which supports strong expression in the embryonic retina within three days of infection (data not shown). We introduced the Fezf1 AAV or control AAVs at E14.5, after nearly all SACs had been born but prior to their segregation. As expected, 3xHA-Fezf1 was detected in the nuclei of infected cells (Figure S2F). SACs infected with control AAVs were equally likely to reside in either the INL or the GCL. In contrast, approximately three times as many cells infected with the Fezf1 AAV were present in the GCL compared with the INL (Figures 2F and 2G). This GCL-biased location induced by Fezf1 overexpression was specific to SACs since other transduced amacrine cells (ChAT/VAChT negative) and horizontal cells remained in their appropriate locations in the INL (Figure S2F). Additionally, introduction of Fezf1 at P1, after migration was complete, had no effect on the distribution of SACs (Figures 2G and S2E). Together these results demonstrate that *Fezf1* is necessary and sufficient for proper SAC positioning in the GCL.

Fezf1 Promotes the Polarization and Migration of ON Starburst Amacrine Cells

The loss of SACs from the GCL in *Fezf1*$^{GFP/GFP}$ mutants likely results from an effect of Fezf1 on ON SAC migration. Therefore, we next characterized the morphology of migrating wild-type and *Fezf1* mutant SACs. At E14.5, GFP-positive presumptive ON SACs exhibited a similar bipolar morphology in both *Fezf1*$^{GFP/+}$ and *Fezf1*$^{GFP/GFP}$ mice (Figure 3Ai), suggesting that the early bipolar morphology of these SACs is not affected by loss of *Fezf1*. In contrast, one day later at E15.5, GFP-positive SACs differed dramatically between *Fezf1*$^{GFP/+}$ and *Fezf1*$^{GFP/GFP}$ mice (Figure 3Aii). GFP-positive SACs in *Fezf1*$^{GFP/+}$ heterozygotes bore a leading process that penetrated the INBL, whereas GFP-positive SACs in *Fezf1*$^{GFP/GFP}$ mice maintained a prominent apical trailing process. This difference persisted as control ON SACs entered the INBL and began to elaborate dendrites in the nascent IPL (Figures 3Aiii and 3Aiv). Thus, loss of *Fezf1* inverts the polarized morphology of ON SACs (Figure 3B), likely impairing their subsequent migration.

It appeared from these experiments that the morphology of *Fezf1*$^{GFP/GFP}$ mutant ON SACs resembled that of control OFF SACs. To visualize the morphology of ON and OFF SACs, we used a mouse line in which Cre recombinase was inserted into the locus encoding *Megf10*, which is expressed by all SACs (Kay et al., 2012; Figures 1C and 1F). We crossed these mice to a Cre-dependent reporter (*Rosa::mTmG*) and visualized SAC morphology at E16.5. Wild-type ON SACs within the INBL exhibited a basally directed leading process, similar to GFP-positive ON SACs in *Fezf1*$^{GFP/+}$ retinas, whereas wild-type OFF SACs in the ONBL bore a prominent trailing process, similar to GFP-positive mutant ON SACs in *Fezf1*$^{GFP/GFP}$ retinas (Figure S3E).

Fezf1 Represses *Rnd3* Expression to Promote Migration into the INBL

The similarity between migrating *Fezf1* mutant "ON" SACs and wild-type OFF SACs raised the possibility that Fezf1 promotes an ON, or represses an OFF, SAC migratory program. We therefore sought differentially expressed, Fezf1-dependent genes that could account for the distinct polarity and migration of ON and OFF SACs. No obvious candidates were selectively expressed by ON SACs, but *Rnd3*, an atypical Rho family GTPase, was enriched in OFF SACs (Figures 1C, 1F, and S1C). In the cerebral cortex, *Rnd3* regulates interkinetic nuclear migration of neuronal progenitors and promotes neuronal migration (Pacary et al., 2011, 2013). In the embryonic retina, *Rnd3* transcript is not strongly detected in retinal progenitors or radially migrating neurons in the ONBL, but it is highly expressed by differentiating neurons, including SACs, in the INBL (Figures S3A and S3B). Approximately 30% and 50% of *Megf10*-positive SACs express high levels of *Rnd3* (>10 puncta per cell; see STAR Methods) at E14.5 and E15.5, respectively (Figures 3C and S3B). By E16.5, when ON and OFF SACs in the central retina can be distinguished by their position, 85% of OFF SACs, but only 15% of ON SACs, express high levels of *Rnd3*, and *Rnd3* levels in ON SACs continue to decrease over time (Figures 3C, S3B, and S3D). These data suggest

(E) Cell densities of GFP-labeled SACs (GFP$^+$) and ChAT/VAChT-labeled SACs (total) in the GCL, INL, and both layers (ALL) in *Fezf1*$^{GFP/+}$ and in *Fezf1*$^{GFP/GFP}$ retinas. N as in (C).

(F) P14 retina sections transduced with AAVs expressing a control reporter (top) or Fezf1 overexpression construct (bottom), introduced at E14.5. In controls, AAV-expressing SACs (dashed circles) are equally likely to reside in the INL or GCL (top). Fezf1 overexpression biases infected SACs to reside in the GCL (bottom).

(G) Ratios of transduced SACs in the INL to the GCL for the indicated conditions. Bars show mean ± SEM from four to six images from four animals (Fezf1 overexpression and AAV9-hSyn1-shScramble control) or two animals (AAV9-CAG-TdTomato) at E14.5 and also four to ten images from eight animals (Fezf1 overexpression) and five animals (AAV9-hSyn1-shScramble control) at P1.

Scale bars are 20 μm. ***$p < 0.001$ by Student's t test. **$p < 0.01$ by one-way ANOVA with post hoc Tukey honestly significant difference (HSD) test. See also Figure S2.

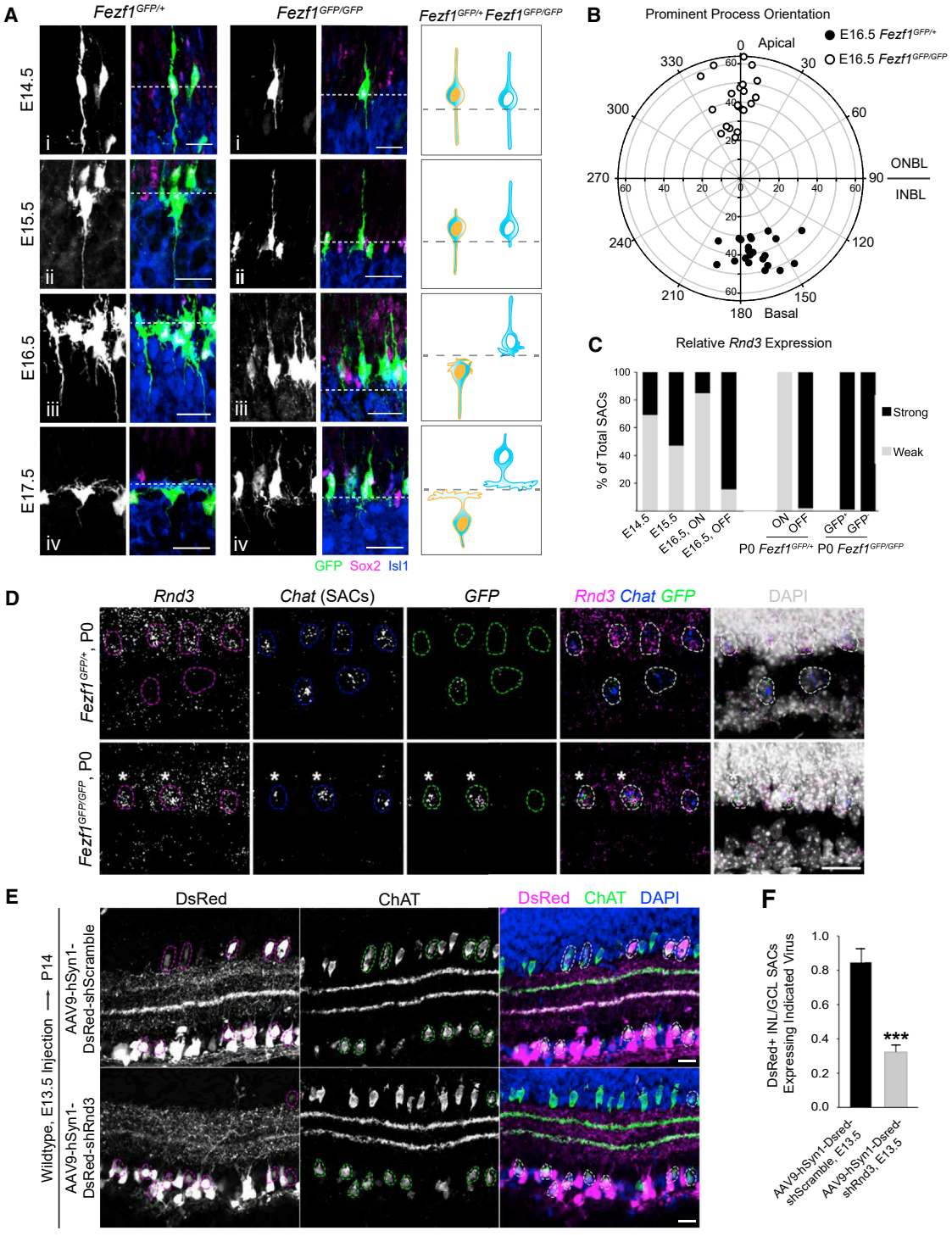

Figure 3. Fezf1 Promotes the Polarization and Migration of ON Starburst Amacrine Cells by Repressing *Rnd3* Expression

(A) GFP-labeled ON SACs (left, middle) and sketches of representative morphologies (right) at indicated embryonic ages in *Fezf1* $^{GFP/+}$ and *Fezf1*$^{GFP/GFP}$ retinas. Embryonic SACs are identified by co-expression of Sox2 (magenta) and Isl1 (blue).

(B) Polar plot of the angle (radial axes) and length (x/y axes) of the prominent neurite of individual ON SACs in E16.5 *Fezf1* $^{GFP/+}$ and *Fezf1*$^{GFP/GFP}$ retinas.

(C) Percentage of total SACs expressing strong or weak levels of *Rnd3* transcript (defined in STAR Methods) at indicated embryonic ages (left; ON and OFF SACs are quantified separately at E16.5 on the basis of the differential positioning of their somata across the IPL) (see Figure S3B for representative images) and in P0 *Fezf1*$^{GFP/+}$ and *Fezf1*$^{GFP/GFP}$ retinas (right).

(legend continued on next page)

that *Rnd3* is upregulated in OFF SACs and downregulated in ON SACs prior to ON SAC migration into the INBL. Moreover, triple FISH against *Rnd3*, *Chat* (all SACs), and *GFP* (ON SACs) revealed that *Rnd3* was upregulated in *Fezf1*$^{GFP/GFP}$ mutant "ON" SACs in the INL (Figures 3C and 3D).

These results suggest that *Rnd3* could confine OFF SACs within the ONBL and, conversely, that loss of *Rnd3* enables SAC migration into the INBL. To test this idea, we generated AAV9 vectors expressing DsRed and either a short hairpin RNA that potently knocked down *Rnd3* expression (*shRnd3*) in heterologous cells (Figure S3C), or a scrambled sequence (*shScramble*), both driven by the hSyn1 promoter. AAVs were introduced intravitreally at E13.5, and retinas were analyzed at P14. In retinas expressing *shRnd3*, the ratio of DsRed-positive SACs in the INL to GCL decreased by 60% compared with retinas expressing *shScramble* (Figures 3E and 3F). Taken together, these data show that *Fezf1* represses *Rnd3* in ON SACs and that this repression enables their entry into the INBL (Figure S3F).

Fezf1 Is Required for ON Starburst Amacrine Cell Fate Specification

Finally, we asked whether the role of Fezf1 in SACs is solely to control their migratory program or if it plays a more general role in specifying SAC fate. We used two approaches, one histological and one molecular, to distinguish between these alternatives.

First, we took advantage of a feature exhibited by most retinal neurons called "mosaic spacing," in which neurons of a single type are more evenly separated from other neurons of the same type than would be expected from a random distribution, whereas they are randomly spaced with respect to neurons of other types (Reese and Keeley, 2015; Wässle and Riemann, 1978). This spacing has been viewed as an indicator that these non-randomly spaced neurons belong to a single type (Rockhill et al., 2000; Sanes and Zipursky, 2010). Both ON and OFF SACs form mosaics in the GCL and INL, respectively (Whitney et al., 2014). Using statistical methods to assess mosaicism (Kay et al., 2012; Reese and Keeley, 2015; Rodieck 1991), we asked if mutant "ON" SACs (ChAT/VAChT and GFP positive) and OFF SACs (ChAT/VAChT positive, GFP negative) together form a single mosaic in the INL of *Fezf1*$^{GFP/GFP}$ retinas. As expected from the increased SAC density in the *Fezf1*$^{GFP/GFP}$ mutant INL (Figure 2D), the exclusion zone radius (spacing between SACs) was reduced in mutants, but their packing pattern and the regularity of their packing did not differ significantly between *Fezf1*$^{GFP/+}$ and *Fezf1*$^{GFP/GFP}$ retinas (Figures S4A and S4B). Thus, by this criterion OFF SACs and GFP-positive mutant "ON" SACs in the INL are members of a single type.

Second, and more directly, we used FACS to isolate GFP-positive SACs from *Fezf1*$^{GFP/+}$ and *Fezf1*$^{GFP/GFP}$ retinas at E17.5 and performed RNA-seq to compare their transcriptomes. The two populations were similar but formed distinct groups (Figures 4A and S4C). Genes common to ON and OFF SACs, as judged by our initial scRNA-seq analysis (Figure 1), were present at similar levels in heterozygotes and homozygous mutants (e.g., *Sox2* and *Megf10*; Figure S4D). However, genes selectively expressed by control ON SACs (ON genes) were downregulated in mutant compared with control GFP-positive SACs, and genes selectively expressed by OFF SACs (OFF genes) were upregulated in the mutant "ON" SACs (Figure 4B). The difference was consistent across replicates, as shown by a composite index based on expression of ON and OFF genes (Figure 4C; see STAR Methods). Consistent with the RNA-seq data, ON SAC markers *Gfra3* and *Slit2* were absent from mutant GFP-positive "ON" SACs, and their expression levels mirrored those observed in GFP-negative OFF SACs (Figures 4D, 4E, S4E, and S4F). Conversely, the mutant "ON" SACs expressed high levels of the OFF SAC-specific gene *Tenm3* (Figures 4F and 4G), in addition to *Rnd3* (Figures 3C and 3D).

Finally, we used triple-label *in situ* hybridization to determine if differential expression of ON and OFF genes is established by E15.5, prior to the time when ON and OFF SACs acquire their distinct positions. We used *Megf10* to label all SACs and *Fezf1* to label presumptive ON SACs. Three OFF SAC-enriched genes (*Tenm3*, *Zfhx3*, and *Cygb*) are selectively expressed in the *Fezf1*-negative presumptive OFF SACs at this stage (Figures S4G and S4H). These results demonstrate that multiple molecular distinctions between ON and OFF SACs are established prior to, and therefore do not depend on, their final positions. On the basis of these results, we conclude that Fezf1 specifies the ON SAC fate by promoting the expression of ON genes and repressing the expression of OFF genes (Figure 4H).

DISCUSSION

A promising strategy for elucidating mechanisms underlying neuronal cell type diversification is to analyze pairs of neurons that are similar in many respects but differ in a key feature. Here, we applied this strategy to a paramorphic retinal pair: ON and OFF SACs. We demonstrate that ON and OFF SACs are transcriptionally distinct cell types prior to their somatic migration, dendritic stratification, and synapse formation. We show that one differentially expressed gene, the transcriptional regulator *Fezf1*, is a critical ON SAC fate determinant, and another differentially expressed gene, the Rho GTPase *Rnd3*, is regulated by Fezf1 to control the differential migration of the SAC types.

(D) *Rnd3*, *Chat*, and *GFP* expression in SACs from P0 *Fezf1* $^{GFP/+}$ and *Fezf1*$^{GFP/GFP}$ retinas detected by RNAscope FISH. Circles outline SACs, and mutant "ON" SACs are *GFP and Chat* positive (asterisk).

(E) P14 retina sections transduced with AAVs expressing control (*shScramble*, top), or *shRnd3* (bottom) hairpins introduced at E13.5. DsRed marks AAV-transduced cells.

(F) Ratios of transduced SACs in the INL compared with the GCL for the indicated conditions. Bars show mean ± SEM from four to ten images from three animals per condition.

Scale bars are 20 μm. ***$p < 0.001$ by Student's t test. See also Figure S3.

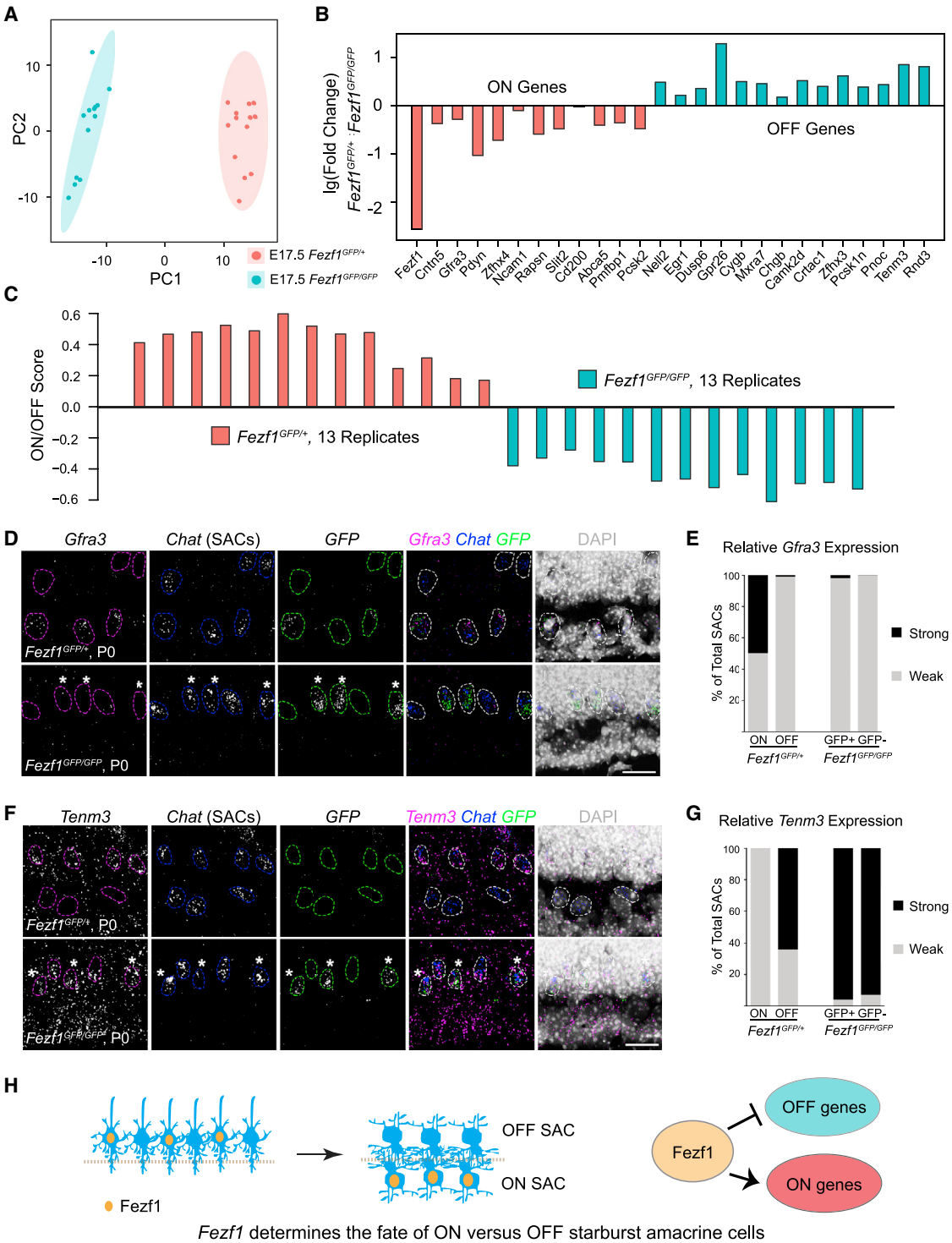

Figure 4. *Fezf1* Is Required for ON Starburst Amacrine Cell Fate Specification

(A) PCA plot of E17.5 *Fezf1* $^{GFP/+}$ and *Fezf1*$^{GFP/GFP}$ ON SAC RNA-seq samples using 400 DE genes.

(B) Expression differences (lg transformation) of ON and OFF genes identified in the P0 SAC scRNA-seq dataset (Figures 1E and 1F) between *Fezf1* $^{GFP/+}$ and *Fezf1*$^{GFP/GFP}$ ON SACs.

(C) ON/OFF score of 13 *Fezf1*$^{GFP/+}$ and *Fezf1*$^{GFP/GFP}$ RNA-seq replicates (see STAR Methods).

(D) RNAscope FISH using *Gfra3*, *Chat*, and *GFP* probes in P0 *Fezf1* $^{GFP/+}$ and *Fezf1*$^{GFP/GFP}$ retinas. Circles outline SACs, and mutant "ON" SACs are *GFP* and *Chat* positive (asterisk).

(legend continued on next page)

Postmitotic Starburst Amacrine Cell Fates Are Determined by Fezf1

Several lines of evidence support the conclusion that Fezf1 controls a postmitotic ON/OFF SAC fate switch. First, *Fezf1* expression is detected only after SACs are born but before they migrate to distinct locations. Second, *Fezf1* is expressed in ON SACs, but not in OFF SACs or any other cell types prior to P6, at which time it appears in a subset of bipolar cells. Last, Fezf1 promotes the expression of ON genes while suppressing OFF genes but does not affect expression of genes shared by ON and OFF SACs. Therefore, *Fezf1* joins a small number of genes shown to control a binary postmitotic cell fate choice (Jukam and Desplan, 2010).

A major outstanding question is how half of the newly postmitotic SACs "choose" to express *Fezf1*. We envision several possibilities. One is that the choice is stochastic, as has been observed in several neuronal and nonneural cell types. Frequently such choices result from the amplification of a small difference by a cell-intrinsic feedback mechanism (Johnston and Desplan, 2010). Another is that extrinsic factors—for example, proximity to another SAC or other cues in the extracellular environment—could affect the choice. A third possibility is that a shared progenitor undergoes an asymmetric terminal division, leading to unequal inheritance of a Fezf1 regulator by daughters (Tajbakhsh et al., 2009). Finally, we cannot rule out the possibility that ON and OFF SACs arise from separate progenitor types, one of which expresses undetectably low levels of *Fezf1*, or is specified to upregulate *Fezf1* postmitotically. We believe that this is unlikely, however, because in a prior analysis of retinal cell lineage (De la Huerta et al., 2012), we observed some clones that contained both ON and OFF SACs.

How Does Fezf1 Regulate Gene Expression in ON Starburst Amacrine Cells?

Fezf1 is a transcriptional repressor that interacts with Groucho/TLE (transducin-like enhancer of split)-type transcriptional corepressors via its EH1 (engrailed homology 1) repressor motif (Shimizu and Hibi, 2009; Shimizu et al., 2010). We found that Fezf1 not only suppresses the expression of OFF genes but also activates the expression of ON genes. How might Fezf1 activate ON genes? One possibility is that Fezf1 derepresses an ON gene transcriptional activator, similar to derepression of neurogenin 2 by Fezf1 and Fezf2 during cortical development (Shimizu et al., 2010). Another possibility is that Fezf1 can function as an activator as well as a repressor, activating ON genes and repressing OFF genes in ON SACs, similar to the way in which Fezf2 determines the cell fate of subcerebral projection neurons by repressing Satb2 and activating Ctip2 expression (Chen et al., 2008). This could be accomplished by context-dependent association of Fezf1 with downstream coactivators and corepressors, respectively. Intriguing candidates here are the zinc finger transcription factors Zfhx3 and Zfhx4, which are selectively expressed by OFF and ON SACs, respectively. Both are predicted to have Fezf1 binding sites (GeneHancer ID: GH16J073045, GH08J076680). Zfhx3 and Zfhx4 are most closely related to each other among the four zinc finger homeobox family members, and their spatial and temporal expression patterns in the brain are consistent with cooperative function in neuronal differentiation (Kostich and Sanes, 1995; Nogami et al., 2005).

Rnd3 Regulation of Starburst Amacrine Cell Polarity and Migration

The *Fezf1*^{GFP} allele allowed us to compare ON (*Fezf1*$^{GFP/+}$) and converted OFF (*Fezf1*$^{GFP/GFP}$) SAC migratory morphologies. Strikingly, we observed that ON and OFF SACs establish prominent neurites of opposite polarity before moving to their final destinations. Rnd3 is an attractive candidate regulator of this difference. Rnd3 lacks intrinsic GTPase activity and remains constitutively active, mediating rearrangement of the actin cytoskeleton by inhibiting the RhoA effector ROCK1 (Jie et al., 2015). In cultured hippocampal neurons, loss of *Rnd3* impairs neuronal polarization and neurite outgrowth (Peris et al., 2012). Strong expression of *Rnd3* by OFF but not ON SACs is consistent with Rnd3 regulating OFF SAC polarity.

Alternatively, Rnd3 may control other aspects of SAC migration. In the mouse neocortex, Rnd3 promotes neuronal radial migration through the cortical plate (Pacary et al., 2011). Given its role in radial migration, it was surprising to see high levels of *Rnd3* in postmitotic neurons in the INBL rather than in radially migrating neurons in the ONBL. This raises the possibility that Rnd3 affects the local positioning of OFF SACs, rather than their radial migration, per se. It is also possible that Rnd3 promotes neurite outgrowth in OFF SACs as a prerequisite for the development of their somal-layer neurite network. This network of connected OFF SACs forms as early as E16 and depends on homotypic contacts mediated by Megf10 (Ray et al., 2018). Therefore, the somal neurite network could stabilize OFF SACs in the ONBL while Fezf1 represses Rnd3 in ON SACs, allowing their migration into the INBL. Consistent with this idea, *Rnd3* expression in ON SACs decreases over time, and knocking down *Rnd3* biases SACs to reside in the GCL.

From Cell Fate Determination to the Assembly of ON and OFF Circuits

Our RNA-seq analysis demonstrated that Fezf1 not only controls initial differences between ON and OFF SACs but also instructs the early expression of adhesion molecules that later pattern the formation of ON and OFF circuits. For instance, Fezf1 promotes expression of Cntn5 in ON SACs, and Cntn5 mediates the formation of ON circuits via homophilic interactions between ON SAC dendrites and ON dendrites of ON-OFF direction-selective

(E) Percentage of total SACs expressing strong or weak levels of *Gfra3* in P0 *Fezf1* $^{GFP/+}$ and *Fezf1*$^{GFP/GFP}$ retinas.
(F) RNAscope FISH using *Tenm3*, *Chat*, and *GFP* probes in P0 *Fezf1* $^{GFP/+}$ and *Fezf1*$^{GFP/GFP}$ retinas.
(G) Percentage of total SACs expressing strong or weak levels of *Tenm3* in P0 *Fezf1* $^{GFP/+}$ and *Fezf1*$^{GFP/GFP}$ retinas.
(H) Model of ON SAC cell fate determination by Fezf1. Fezf1 inhibits OFF genes while promoting ON genes (see Discussion).
Scale bars are 20 μm. See also Figure S4.

ganglion cells (ooDSGCs) (Peng et al., 2017). Additional intriguing candidate genes downstream of Fezf1 are *Slit2* and *Teneurin-3* (*Tenm3*), both of which are predicted to have Fezf1 binding sites (GH041020276 and GH04J182175). *Slit2* is enriched in ON SACs, while *Tenm3* is selectively expressed by OFF SACs. However, published images suggest that *Slit2* does not affect SAC lamination (Rama et al., 2015), and our preliminary data do not support a role for *Tenm3* in this process (data not shown). It remains possible that either or both might be involved, like Cntn5, in mediating interactions between SACs and their synaptic partners.

STAR★METHODS

Detailed methods are provided in the online version of this paper and include the following:

- KEY RESOURCES TABLE
- LEAD CONTACT AND MATERIALS AVAILABILITY
- EXPERIMENTAL MODEL AND SUBJECT DETAILS
  - Mice
  - Chicken and Marmoset
- METHOD DETAILS
  - Single Cell Isolation and Droplet Based scRNA-seq
  - RNA-seq of SACs from Fezf1 Mutants via Smart-seq2
  - ScRNA-seq Data Analysis
  - Tissue Processing and Fluorescent *In Situ* Hybridization
  - RNAscope *In Situ* Hybridization
  - Immunohistochemistry
  - Image Acquisition and analysis
  - Generation and use of AAV vectors
- QUANTIFICATION AND STATISTICAL ANALYSIS
- DATA AND CODE AVAILABILITY

SUPPLEMENTAL INFORMATION

Supplemental Information can be found online at https://doi.org/10.1016/j.neuron.2019.11.002.

ACKNOWLEDGMENTS

This work was supported by NIH grant R37NS029169-29 (J.R.S.), funding from the Howard Hughes Medical Institute (A.L.K.), and NIH Visual Science Training Program (VSTP) grants 5T32EY007143-20 and F32EY025114 (R.E.J.). We are grateful to Dr. Bin Chen (University of California, Santa Cruz) for generously providing Fezf1^{GFP} mutant mice. We thank Drs. Loyal A. Goff and Karthik Shekhar for advice on scRNA-seq analysis strategies. We thank Mallory Laboulaye at Harvard and Nicole Kropowski, Randal Hand, Natalie Hamilton, and Tim Al-Khindi at Johns Hopkins for technical assistance. We also thank members of the J.R.S. and A.L.K. laboratories for helpful discussions and comments on the manuscript.

AUTHOR CONTRIBUTIONS

R.E.J., A.L.K., Y.-R.P., and J.R.S. conceived and designed experiments, analyzed data, and wrote the paper. R.E.J. and Y.-R.P. performed experiments. J.N.K. generated the Megf10-Cre allele. W.Y. analyzed data.

DECLARATION OF INTERESTS

The authors declare no competing interests

Received: June 10, 2019
Revised: October 7, 2019
Accepted: October 30, 2019
Published: December 4, 2019

REFERENCES

Buffelli, M., Burgess, R.W., Feng, G., Lobe, C.G., Lichtman, J.W., and Sanes, J.R. (2003). Genetic evidence that relative synaptic efficacy biases the outcome of synaptic competition. Nature *424*, 430–434.

Chen, B., Wang, S.S., Hattox, A.M., Rayburn, H., Nelson, S.B., and McConnell, S.K. (2008). The Fezf2-Ctip2 genetic pathway regulates the fate choice of subcortical projection neurons in the developing cerebral cortex. Proc. Natl. Acad. Sci. U S A *105*, 11382–11387.

De la Huerta, I., Kim, I.J., Voinescu, P.E., and Sanes, J.R. (2012). Direction-selective retinal ganglion cells arise from molecularly specified multipotential progenitors. Proc. Natl. Acad. Sci. U S A *109*, 17663–17668.

Eckler, M.J., and Chen, B. (2014). Fez family transcription factors: controlling neurogenesis and cell fate in the developing mammalian nervous system. BioEssays *36*, 788–797.

Eckler, M.J., McKenna, W.L., Taghvaei, S., McConnell, S.K., and Chen, B. (2011). Fezf1 and Fezf2 are required for olfactory development and sensory neuron identity. J. Comp. Neurol. *519*, 1829–1846.

Famiglietti, E.V., Jr. (1983). 'Starburst' amacrine cells and cholinergic neurons: mirror-symmetric on and off amacrine cells of rabbit retina. Brain Res. *261*, 138–144.

Famiglietti, E.V. (2004). Class I and class II ganglion cells of rabbit retina: a structural basis for X and Y (brisk) cells. J. Comp. Neurol. *478*, 323–346.

Famiglietti, E.V. (2005). "Small-tufted" ganglion cells and two visual systems for the detection of object motion in rabbit retina. Vis. Neurosci. *22*, 509–534.

Finak, G., McDavid, A., Yajima, M., Deng, J., Gersuk, V., Shalek, A.K., Slichter, C.K., Miller, H.W., McElrath, M.J., Prlic, M., et al. (2015). MAST: a flexible statistical framework for assessing transcriptional changes and characterizing heterogeneity in single-cell RNA sequencing data. Genome Biol. *16*, 278.

Hand, R., Bortone, D., Mattar, P., Nguyen, L., Heng, J.I., Guerrier, S., Boutt, E., Peters, E., Barnes, A.P., Parras, C., et al. (2005). Phosphorylation of Neurogenin2 specifies the migration properties and the dendritic morphology of pyramidal neurons in the neocortex. Neuron *48*, 45–62.

Hand, R.A., Khalid, S., Tam, E., and Kolodkin, A.L. (2015). Axon Dynamics during Neocortical Laminar Innervation. Cell Reports *12*, 172–182.

Heinze, L., Harvey, R.J., Haverkamp, S., and Wässle, H. (2007). Diversity of glycine receptors in the mouse retina: localization of the alpha4 subunit. J. Comp. Neurol. *500*, 693–707.

Jie, W., Andrade, K.C., Lin, X., Yang, X., Yue, X., and Chang, J. (2015). Pathophysiological Functions of Rnd3/RhoE. Compr. Physiol. *6*, 169–186.

Johnston, R.J., Jr., and Desplan, C. (2010). Stochastic mechanisms of cell fate specification that yield random or robust outcomes. Annu. Rev. Cell Dev. Biol. *26*, 689–719.

Jukam, D., and Desplan, C. (2010). Binary fate decisions in differentiating neurons. Curr. Opin. Neurobiol. *20*, 6–13.

Kaneda, M., Ito, K., Shigematsu, Y., and Shimoda, Y. (2010). The OFF-pathway dominance of P2X(2)-purinoceptors is formed without visual experience. Neurosci. Res. *66*, 86–91.

Kay, J.N., Chu, M.W., and Sanes, J.R. (2012). MEGF10 and MEGF11 mediate homotypic interactions required for mosaic spacing of retinal neurons. Nature *483*, 465–469.

Knabe, W., Washausen, S., Happel, N., and Kuhn, H.J. (2007). Development of starburst cholinergic amacrine cells in the retina of Tupaia belangeri. J. Comp. Neurol. *502*, 584–597.

Kostich, W.A., and Sanes, J.R. (1995). Expression of zfh-4, a new member of the zinc finger-homeodomain family, in developing brain and muscle. Dev. Dyn. *202*, 145–152.

Muzumdar, M.D., Tasic, B., Miyamichi, K., Li, L., and Luo, L. (2007). A global double-fluorescent Cre reporter mouse. Genesis *45*, 593–605.

Nogami, S., Ishii, Y., Kawaguchi, M., Sakata, N., Oya, T., Takagawa, K., Kanamori, M., Sabit, H., Obata, T., Kimura, T., and Sasahara, M. (2005). ZFH4 protein is expressed in many neurons of developing rat brain. J. Comp. Neurol. *482*, 33–49.

Pacary, E., Heng, J., Azzarelli, R., Riou, P., Castro, D., Lebel-Potter, M., Parras, C., Bell, D.M., Ridley, A.J., Parsons, M., and Guillemot, F. (2011). Proneural transcription factors regulate different steps of cortical neuron migration through Rnd-mediated inhibition of RhoA signaling. Neuron *69*, 1069–1084.

Pacary, E., Azzarelli, R., and Guillemot, F. (2013). Rnd3 coordinates early steps of cortical neurogenesis through actin-dependent and -independent mechanisms. Nat. Commun. *4*, 1635.

Peng, Y.R., Tran, N.M., Krishnaswamy, A., Kostadinov, D., Martersteck, E.M., and Sanes, J.R. (2017). Satb1 regulates contactin 5 to pattern dendrites of a mammalian retinal ganglion cell. Neuron *95*, 869–883.e6.

Peng, Y.R., Shekhar, K., Yan, W., Herrmann, D., Sappington, A., Bryman, G.S., van Zyl, T., Do, M.T.H., Regev, A., and Sanes, J.R. (2019). Molecular classification and comparative taxonomics of foveal and peripheral cells in primate retina. Cell *176*, 1222–1237.e22.

Peris, B., Gonzalez-Granero, S., Ballester-Lurbe, B., García-Verdugo, J.M., Pérez-Roger, I., Guerri, C., Terrado, J., and Guasch, R.M. (2012). Neuronal polarization is impaired in mice lacking RhoE expression. J. Neurochem. *121*, 903–914.

Picelli, S., Faridani, O.R., Björklund, A.K., Winberg, G., Sagasser, S., and Sandberg, R. (2014). Full-length RNA-seq from single cells using Smart-seq2. Nat. Protoc. *9*, 171–181.

Rama, N., Dubrac, A., Mathivet, T., Ní Chárthaigh, R.A., Genet, G., Cristofaro, B., Pibouin-Fragner, L., Ma, L., Eichmann, A., and Chédotal, A. (2015). Slit2 signaling through Robo1 and Robo2 is required for retinal neovascularization. Nat. Med. *21*, 483–491.

Ray, T.A., Roy, S., Kozlowski, C., Wang, J., Cafaro, J., Hulbert, S.W., Wright, C.V., Field, G.D., and Kay, J.N. (2018). Formation of retinal direction-selective circuitry initiated by starburst amacrine cell homotypic contact. eLife *7*, e34241.

Reese, B.E., and Keeley, P.W. (2015). Design principles and developmental mechanisms underlying retinal mosaics. Biol. Rev. Camb. Philos. Soc. *90*, 854–876.

Rockhill, R.L., Euler, T., and Masland, R.H. (2000). Spatial order within but not between types of retinal neurons. Proc. Natl. Acad. Sci. U S A *97*, 2303–2307.

Rodieck, R.W. (1991). The density recovery profile: a method for the analysis of points in the plane applicable to retinal studies. Vis. Neurosci. *6*, 95–111.

Rossi, J., Balthasar, N., Olson, D., Scott, M., Berglund, E., Lee, C.E., Choi, M.J., Lauzon, D., Lowell, B.B., and Elmquist, J.K. (2011). Melanocortin-4 receptors expressed by cholinergic neurons regulate energy balance and glucose homeostasis. Cell Metab. *13*, 195–204.

Rousso, D.L., Qiao, M., Kagan, R.D., Yamagata, M., Palmiter, R.D., and Sanes, J.R. (2016). Two pairs of ON and OFF retinal ganglion cells are defined by intersectional patterns of transcription factor expression. Cell Rep. *15*, 1930–1944.

Sanes, J.R., and Zipursky, S.L. (2010). Design principles of insect and vertebrate visual systems. Neuron *66*, 15–36.

Shekhar, K., Lapan, S.W., Whitney, I.E., Tran, N.M., Macosko, E.Z., Kowalczyk, M., Adiconis, X., Levin, J.Z., Nemesh, J., Goldman, M., et al. (2016). Comprehensive classification of retinal bipolar neurons by single-cell transcriptomics. Cell *166*, 1308–1323.e30.

Shimizu, T., and Hibi, M. (2009). Formation and patterning of the forebrain and olfactory system by zinc-finger genes Fezf1 and Fezf2. Dev. Growth Differ. *51*, 221–231.

Shimizu, T., Nakazawa, M., Kani, S., Bae, Y.K., Shimizu, T., Kageyama, R., and Hibi, M. (2010). Zinc finger genes Fezf1 and Fezf2 control neuronal differentiation by repressing Hes5 expression in the forebrain. Development *137*, 1875–1885.

Stacy, R.C., and Wong, R.O. (2003). Developmental relationship between cholinergic amacrine cell processes and ganglion cell dendrites of the mouse retina. J. Comp. Neurol. *456*, 154–166.

Tajbakhsh, S., Rocheteau, P., and Le Roux, I. (2009). Asymmetric cell divisions and asymmetric cell fates. Annu. Rev. Cell Dev. Biol. *25*, 671–699.

Thangaraj, G., Greif, A., Bachmann, G., and Layer, P.G. (2012). Intricate paths of cells and networks becoming "Cholinergic" in the embryonic chicken retina. J. Comp. Neurol. *520*, 3181–3193.

Trapnell, C., Roberts, A., Goff, L., Pertea, G., Kim, D., Kelley, D.R., Pimentel, H., Salzberg, S.L., Rinn, J.L., and Pachter, L. (2012). Differential gene and transcript expression analysis of RNA-seq experiments with TopHat and Cufflinks. Nat. Protoc. *7*, 562–578.

Usrey, W.M., and Fitzpatrick, D. (1996). Specificity in the axonal connections of layer VI neurons in tree shrew striate cortex: evidence for distinct granular and supragranular systems. J. Neurosci. *16*, 1203–1218.

Vaney, D.I., Sivyer, B., and Taylor, W.R. (2012). Direction selectivity in the retina: symmetry and asymmetry in structure and function. Nat. Rev. Neurosci. *13*, 194–208.

Voinescu, P.E., Kay, J.N., and Sanes, J.R. (2009). Birthdays of retinal amacrine cell subtypes are systematically related to their molecular identity and soma position. J. Comp. Neurol. *517*, 737–750.

Wang, Q., Chiu, S., Koropouli, E., Hong, I., Mitchell, S., Easwaran, T.P., Hamilton, N.R., Gustina, A.S., Zhu, Q., Ginty, D.D., Huganir, R.L., and Kolodkin, A.L. (2017). Neuropilin-2/PlexinA3 Receptors Associate with GluA1 and Mediate Sema3F-dependent Homeostatic Scaling in Cortical Neurons. Neuron *96*, 1084–1098.

Wässle, H., and Riemann, H.J. (1978). The mosaic of nerve cells in the mammalian retina. Proc. R. Soc. Lond. B Biol. Sci. *200*, 441–461.

Whitney, I.E., Keeley, P.W., St John, A.J., Kautzman, A.G., Kay, J.N., and Reese, B.E. (2014). Sox2 regulates cholinergic amacrine cell positioning and dendritic stratification in the retina. J. Neurosci. *34*, 10109–10121.

Zhang, C., Yu, W.Q., Hoshino, A., Huang, J., Rieke, F., Reh, T.A., and Wong, R.O.L. (2019). Development of ON and OFF cholinergic amacrine cells in the human fetal retina. J. Comp. Neurol. *527*, 174–186.

STAR★METHODS

KEY RESOURCES TABLE

REAGENT or RESOURCE	SOURCE	IDENTIFIER
Antibodies		
Chicken polyclonal anti-GFP	Abcam	Cat# ab13970; RRID: AB_300798
Rabbit polyclonal anti-GFP	Millipore	Cat# AB3080P; RRID: AB_2630379
Mouse polyclonal anti-Isl1	DSHB	Cat# 39.4D5; RRID: AB_2314683
Goat polyclonal anti-Choline Acetyltransferase	Millipore	Cat# AB144P; RRID: AB_11214092
Goat polyclonal anti-Vesicular Acetylcholine Transporter	Millipore	Cat# ABN100; RRID: AB_2630394
Goat polyclonal anti-Sox-2 (Y-17)	Santa Cruz	Cat# sc-17320; RRID: AB_2286684
Rabbit polyclonal anti-Dsred	Living Colors	Cat# 632496; RRID: AB_10013483
Chicken polyclonal anti-GFP	AVES	Cat# GFP-1020; RRID: AB_10000240
Rabbit monoclonal anti-HA	Cell Signaling	Cat# 3724s; RRID: AB_1549585
Mouse monoclonal anti-actin, clone C4	Millipore	Cat# MAB1501; RRID: AB_2223041
Chemicals, Peptides, and Recombinant Proteins		
Ames' Medium	Sigma	Cat# A1420
Papain	Worthington	Cat# LS003126
Ovomucoid	Worthington	Cat# LS003087
AzuraQuant cDNA synthesis kit	Azura	Cat# AZ-199
DAPI (4',6-Diamidino-2-Phenylindole, Dihydrochloride)	Life Technologies	Cat# D1306; RRID: AB_2629482
Lipofectamine 2000 Transfection Reagent	Thermo Fisher Scientific	Cat# 11668019
Critical Commercial Assays		
Chromium Single Cell 3′ Library & Gel Bead Kit v2, 16 rxns	10X Genomics	Cat# 120237
Chromium Single Cell A Chip Kit, 16 rxns	10X Genomics	Cat# 1000009
Chromium i7 Multiplex Kit 96 rxns	10X Genomics	Cat# 120262
Smart-seq2 reagents	Picelli et al., 2014	N/A
Nextera XT DNA Library Preparation Kit	Illumina	Cat# FC-131-1024
RNAscope Fluorescent Multiplex Kit	Advanced Cell Diagnostics	Cat# 320850
RNAlater	Thermo Fisher	Cat# AM7024
RNeasy Mini Kit	QIAGEN	Cat# A74104
RNAclean SPRI	Beckman Coulter Genomics	Cat# A63987
RNAscope Probe- eGFP	Advanced Cell Diagnostics	Cat# 400281
RNAscope Probe- GFP-C2	Advanced Cell Diagnostics	Cat# 409011-C2
RNAscope Probe- Mm-Chat-C3	Advanced Cell Diagnostics	Cat# 410071-C3
RNAscope Probe- Mm-Megf10-C3	Advanced Cell Diagnostics	Cat# 406641-C3
RNAscope Probe- Mm-Rnd3-C2	Advanced Cell Diagnostics	Cat# 424731-C2
RNAscope Probe- Mm-Gfra3-C2	Advanced Cell Diagnostics	Cat# 467191-C2
RNAscope Probe- Mm-Slit2-C2	Advanced Cell Diagnostics	Cat# 449691-C2
RNAscope Probe- Mm-Tenm3	Advanced Cell Diagnostics	Cat# 411951
RNAscope 3-plex Negative Control Probe	Advanced Cell Diagnostics	Cat# 320871
RNAscope 3-plex Positive Control Probe Mm	Advanced Cell Diagnostics	Cat# 320881
NEBuilder HiFi DNA Assembly Cloning Kit	New England BioLabs	Cat# E5520S
Phusion Hot Start Flex 2X Master Mix	New England BioLabs	Cat# M0536S

(*Continued on next page*)

Continued

REAGENT or RESOURCE	SOURCE	IDENTIFIER
SuperScript III First-Strand Synthesis SuperMix	Thermo Fisher	Cat# 18080400
TRIzol Plus RNA Purification Kit	Thermo Fisher	Cat# 12183555
Deposited Data		
Raw data files for scRNA-sequencing	This study	GEO: GSE132555
Raw data files for RNA-sequencing	This study	GEO: GSE132555
Experimental Models: Organisms/Strains		
Mouse: *Fezf1:eGFP*	Gift from B. Chen	Jackson Laboratory Stock number 034493
Mouse: B6.Cg-Tg(Thy1-EYFP)15Jrs/J	Buffelli et al., 2003	Jackson Laboratory Stock#: 005630; RRID: IMSR_JAX:005630
Mouse: CD1	Charles River	022
Mouse: *Megf10:Cre*	This paper	N/A
Mouse: B6.129(Cg)-Gt(ROSA) 26Sor$^{tm4(ACTB-tdTomato,-EGFP)Luo}$/J	Jackson Laboratory	Jackson Laboratory Stock#: 007676, RRID: IMSR_JAX:007676
Experimental Models: Cell Lines		
Cell line: HEK293T cells	ATCC	Cat# CRL-3216; RRID: CVCL_0063
Bacterial and Virus Strains		
AAV9-hSyn1-3XHA-Fezf1-P2A-eGFP (4.01E+13)	Janelia Research Campus Viral Tools	N/A
AAV9-CAG-TdTomato (4.01E+13)	UNC Vector Core	N/A
AAV9-DsRed-shScrambled ((4.01E+13)	Janelia Research Campus Viral Tools	N/A
AAV9-hSyn1-DsRed-shRnd3 (4.8393E+13)	Janelia Research Campus Viral Tools	N/A
AAV9-hSyn1-DsRed-shScrambled (4.8393E+13)	Janelia Research Campus Viral Tools	N/A
Recombinant DNA		
pCIG2	Hand et al., 2005	N/A
pCIG2-LSL-3xHA-Fezf1	This study	N/A
pCIG2-LSL-3xHA-Rnd3	This study	N/A
pCAG-Cre	Hand et al., 2015	N/A
pPRIME-DsRed-shScramble	This study	N/A
pPRIME-DsRed-shRnd3	This study	N/A
pAAV-hSyn1-MCS	This study	N/A
pAAV-hSyn1-3xHA-Fezf1-P2A-eGFP	This study	N/A
pAAV-hSyn1-DsRed-shScramble	This study	N/A
pAAV-hSyn1-DsRed-shRnd3	This study	N/A
Oligonucleotides		
See Table S1		N/A
Software and Algorithms		
Cell Ranger v2.1.0	10X genomics	https://support.10xgenomics.com/single-cell-gene-expression/software/downloads/latest
Tophat	Trapnell et al., 2012	RRID: SCR_013035
Cufflinks	Trapnell et al., 2012	http://cole-trapnell-lab.github.io/cufflinks/; RRID: SCR_014597
Cuffdiff	Trapnell et al., 2012	http://cole-trapnell-lab.github.io/cufflinks/; RRID: SCR_001647
R version 3.4.1	The R project	https://www.r-project.org/
ImageJ	NIH	https://imagej.nih.gov/ij/; RRID: SCR_003070
Pairwise stitching ImageJ plugin	NIH	https://imagej.net/Image_Stitching

(*Continued on next page*)

Continued

REAGENT or RESOURCE	SOURCE	IDENTIFIER
Segmentation Simple Neurite Tracer ImageJ plugin	NIH	https://imagej.net/Simple_Neurite_Tracer
DRP	Rockhill et al., 2000	N/A
Zen	Zeiss	RRID:SCR_013672 https://www.zeiss.com/microscopy/en_us/products/microscope-software/zen.html
Other		
Illumina Nextseq 500	Illumina	N/A
Illumina Hiseq	Illumina	N/A

LEAD CONTACT AND MATERIALS AVAILABILITY

Further information and requests for reagents may be directed and will be fulfilled by the lead contact Joshua R. Sanes (sanesj@mcb.harvard.edu).

All unique/stable reagents generated in this study are available from the corresponding authors without restriction.

EXPERIMENTAL MODEL AND SUBJECT DETAILS

All animal experiments were approved by the Institutional Animal Care and Use Committees (IACUC) at Harvard University and The Johns Hopkins University School of Medicine.

Mice

Mice were maintained in pathogen-free facilities at Harvard and Johns Hopkins Universities under standard housing conditions with continuous access to food and water. Timed-pregnant mice were either purchased from Charles River or set up in house. RNA sequencing experiments were carried out at embryonic age (E) 16, 17.5, and postnatal (P) 0. Histological and *in situ* hybridization studies used E14.5 to adult mice as indicated. Mice of both sexes were used, and no sexual dimorphisms were observed in any results reported here. None of the mice had noticeable health or immune status abnormalities and were not subject to prior procedures. The genotype of mice is described where appropriate. The following mouse lines were used:

1. In *Fezf1*^{GFP}, eGFP was inserted into the endogenous *Fezf1* locus, generating a null allele and leading to expression of eGFP in cells that normally express Fezf1 (Eckler et al., 2011).
2. In *ChAT*^{Cre} mice, Cre was inserted downstream of the *ChAT* coding sequence, leading to expression of Cre in cholinergic neurons without disrupting endogenous ChAT expression (Rossi et al., 2011).
3. In *Thy1-stop-YFP* Line #15 transgenic mice, a lox-stop-lox eYFP cassette is expressed under control of regulatory elements from the mouse *Thy1* gene, leading to cre-dependent expression of YFP in many neuronal population (Buffelli et al., 2003).
4. In *Megf10*^{Cre} mice, Cre was inserted in the *Megf10* locus without disrupting endogenous Megf10 expression. A complete description of this line will be presented elsewhere (J.N.K., in preparation). Briefly, Cre recombinase was inserted at the end of the Megf10 coding exon, with the two reading frames separated by a T2A sequence.
5. In *ROSA*$^{mT/mG}$ mice, a lox-membrane-localized tdTomato (mT) - membrane-localized eGFP (mG) cassette was inserted into the *ROSA26* locus. Thus, mG is expressed in cells that express or previously expressed Cre recombinase, while mT is expressed in other cells (Muzumdar et al., 2007).
6. Timed pregnant CD1-IGS mice from Charles River were used for *in situ* hybridization and viral transduction experiments.

Chicken and Marmoset

Specific-Pathogen-Free (SPF) eggs were purchased from Charles River. Eyes were collected from E8 embryos. Eyes from a newborn marmoset (*Callithrix jacchus*) were generously provided by the McGovern Institute for Brain Research (Massachusetts Institute of Technology). We are grateful to G. Feng, Q. Zhang and C. Wu for access to this tissue. Eyes were collected and transported in ice-cold Hibernate-A (BrainBits).

METHOD DETAILS

Single Cell Isolation and Droplet Based scRNA-seq

P0 *ChAT*^{Cre}:*Thy1-STP-YFP* (line#15) retinas were digested with papain (Worthington, LS003126) at 37°C for 10 mins. Retinas were then dissociated and triturated into single cell suspensions. YFP labeled SACs were isolated by FACS and loaded into 10X Chromium

Single Cell A Chips at a concentration of ~1,000 cells/μL. E16 SACs were collected from an unrelated project in which RGCs were targeted, but SACs were also obtained (I. E. Whitney and J.R.S., submitted).

Single cell libraries were prepared using the Chromium 3′ v2 platform (10X Genomics, Pleasanton, CA) as previously described (Peng et al., 2019). Libraries were sequenced on the Illumina HiSeq 2500 (Paired-end reads: Read 1, 26bp, Read 2, 98bp).

RNA-seq of SACs from Fezf1 Mutants via Smart-seq2

E17.5 *Fezf1*$^{GFP/+}$ and *Fezf1*$^{GFP/GFP}$ SACs were isolated by FACS in pools of 100 cells. 13 replicates were collected from mice of each genotype. cDNA libraries were prepared with Smart-seq2 and Nextera XT (Picelli et al., 2014). Libraries were sequenced on the Illumina NextSeq with paired-end 75bp reads.

ScRNA-seq Data Analysis

ScRNA-seq data were analyzed as previously described (Peng et al., 2019; Shekhar et al., 2016). Briefly, sequenced reads were aligned to the mouse genome mm10, and count matrix of sequenced cells was generated using the Cell Ranger software (version 2.1.0, 10X Genomics). Only cells with the expression of >600 genes were used for further analysis. We preprocessed the count data following normalization to median UMI counts, regressing out (removing correlations associated with expression strength) mitochondrial and ribosome genes, and extraction of all the SACs with scoring for gene signatures of SACs – *Sox2*, *Megf10*, *Megf11*, *Chat*, and *Slc18a3*. Lastly, we clustered SACs with graph-based clustering using significant PCs and visualized the clustering result in 2D via t-distributed stochastic neighbor embedding (t-SNE). Differential expression (DE) tests for a gene between two identified clusters (later validated as ON and OFF SAC clusters) were performed using the 'MAST' package with the criteria of at least expression at 20% cells within a cluster and threshold of 0.25 (Finak et al., 2015).

RNA-seq data were analyzed as previously described (Peng et al., 2017). Briefly, sequenced reads were mapped to the mouse genome (mm10) via Tophat (Trapnell et al., 2012); transcripts were counted via Cufflinks; differentially expressed genes were detected with Cuffdiff.

ON/OFF scores of all 26 replicates were calculated with a log2 transformation of the ratio of average expression levels of ON genes to that of OFF genes.

Tissue Processing and Fluorescent *In Situ* Hybridization

Timed-pregnant mice were anesthetized with intraperitoneal injection of euthasol (Virbac), and eyes from embryos were collected and fixed in 4% PFA for 1hr at 4°C. Retinas were then dissected and fixed with 4% PFA for additional 0.5hr at 4°C. Eyes were collected from P0-P8 mice after cervical dislocation and from adults euthanized with intraperitoneal injection of euthasol. Retinas were dissected and fixed with 4% PFA for 1.5-2hr at 4°C. E8 chicken eyes were collected and fixed with 4% PFA for 1hr at 4°C, and retinas were dissected and further fixed with 4% PFA for 0.5 hr at 4°C. Marmoset retinas were dissected in Ames from newborn marmoset eyes and fixed with 4% PFA overnight at 4°C.

After fixation, retinas were rinsed with PBS, immersed with 30% sucrose overnight at 4°C, embedded in Tissue Freezing Medium (EMS) and cryosectioned at 20 μm on Superfrost Plus slides (Fisher).

Probe templates were generated using cDNA derived from mouse, chicken, and marmoset retinas following RNA extraction and reverse transcription with AzuraQuant cDNA Synthesis Kit (Azura, AZ-1995). Antisense probes were generated by PCR using a reverse primer with a T7 sequence adaptor to permit *in vitro* transcription (see Key Resources Table for primer sequences). DIG rUTP (Roche, 11277073910), DNP rUTP (Perkin Elmer, NEL555001EA), and Fluorescein rUTP (Roche, 11685619910) were used for synthesizing probes for double fluorescent *in situ* hybridization (FISH) experiments. Details of FISH were previously described (Peng et al., 2019; Shekhar et al., 2016). Briefly, retinal sections were treated with 1.5 μg/ml of proteinase K (NEB, P8107S) and then post-fixed and treated with acetic anhydride for deacetylation. Probe detection was performed with anti-DIG HRP (1:1000) and anti-Fluorescein (1:1000) or anti-DNP HRP (1:500) followed by tyramide amplification.

RNAscope *In Situ* Hybridization

Timed-pregnant mice were euthanized by continuous exposure to CO_2 followed by cervical dislocation. Embryos were harvested and decapitated, and eyes were dissected and fixed overnight in RNase-free 4% PFA with rotation. Eyes were rinsed twice for 20 min in RNase-free PBS, followed by RNase-free 15% sucrose at room temperature for 1-2 h, until the eyes sunk. They were then immersed in RNase-free 30% sucrose overnight, embedded in Neg-50 (Thermo Scientific) mounting medium, and cryosectioned at 14 μm onto Superfrost Plus slides (Fisher). Slides were stored at −80°C until use.

Slides were thawed from −80°C, dried for 20 min at room temperature, and then baked at 60°C for 1 h prior to target retrieval. The RNAscope assay was then conducted per the manufacturer's protocol with the following modifications: 1) during the target retrieval step, the slides were slowly inserted into target retrieval solution at 90-95°C for 2 min and 30 s; 2) slides were incubated in DAPI in the final step for 2.5 min. Protease III was used.

Images were acquired with a 40X EC Plan Apochromat NA1.3 oil immersion objective (Zeiss) at the resolution of 1024x1024 pixels and Z-step size of 0.5-0.75 μm, 6-12 slices per image to encompass the entirety of the mRNA signal. To score number of mRNA puncta per cell, outlines of individual SACs were drawn on the image with the segmented line tool in ImageJ using the *Megf10* (embryonic *Rnd3* experiments) or *Chat* (P0 *Fezf1*$^{GFP/GFP}$ mutant quantifications) and DAPI channels. Cells were grouped into expression

bins based on the relative numbers of puncta per gene of interest while scrolling through each optical section, rather than in a Z-projection, to enhance binning accuracy. Bins were determined for each gene separately owing to their different levels of expression. The following bins were used:

Gene	Weak Expression (n puncta)	Strong Expression (n puncta)
Rnd3 (all quantifications)	≤10	> 10
Gfra3	≤3	> 3
Tenm3	≤10	> 10
Slit2	≤3	> 3

The quantification of embryonic *Rnd3* expression was performed blinded. Since the *Fezf1*$^{GFP/GFP}$ phenotype was visible, a blinded analysis of this phenotype was infeasible.

Immunohistochemistry

Retinal tissues were prepared as described above. Antibodies used were as follows: chick and rabbit anti-GFP (1:500, Abcam; 1:5000, Millipore; 1:1000, AVES); goat anti-choline acetyltransferase (1:500, Millipore); goat anti-VAChT (1:1000, Millipore); goat anti-Sox2 (1:100, Santa Cruz); mouse anti-Isl1 (1:10, DSHB), rabbit anti-HA (1:500, Cell Signaling), and rabbit anti-DsRed (1:1000, Living Colors), and mouse anti-Ki67 (1:200, BD Biosciences). Nuclei were labeled with DAPI (1:1000, Invitrogen). Secondary antibodies were conjugated to Alexa Fluor 488, 568, and 647 (Invitrogen) and used at 1:1000. Fluoromount-G (SouthernBiotech) was used for mounting wholemounts. ProLong Gold Antifade was used for mounting retina section slides.

Image Acquisition and analysis

Images were acquired on Zeiss LSM 710 confocal microscopes with 405, 488-515, 568, and 647 lasers, processed using Zeiss ZEN software, and analyzed using ImageJ (NIH). Section images were acquired with 10X, 16X, 40X or 63X oil lens at the resolution of 1024x1024 pixels, a step size of 0.5-1.5 μm. ImageJ (NIH) software was used to generate maximum intensity projections. Adobe Photoshop CC was used for adjustments to brightness and contrast.

Generation and use of AAV vectors

Fezf1 Overexpression

The *Fezf1* coding sequence (CDS) was amplified from a P3 retinal cDNA library (RNA was extracted using the Invitrogen TRIzol Plus RNA Purification Kit and reverse transcribed using Invitrogen SuperScript III First-Strand Synthesis SuperMix). Using NEBuilder® HiFi DNA Assembly kit, we ligated a 3x-Hemagglutinin (HA) tag to the N terminus of the Fezf1 CDS. We then cloned the *3xHA-Fezf1* fragment into a modified pCIG2 plasmid (Hand et al., 2005), which we modified to include a Lox-STOP-Lox (Hand et al., 2015) cassette to allow Cre-dependent expression of Fezf1. Using pCAG-Cre (Hand et al., 2015), we examined expression of pCIG2-LSL-3xHA-Fezf1 in HEK293T cell, and detected specific HA signal in the nucleus with anti-HA antibody staining (data not shown). This strategy was also used to make a Cre-dependent Rnd3 overexpression construct — pCIG2-LSL-3xHA-Rnd3 (see below). We next designed an ultramer containing a furin cleavage site plus linker (RAKR-SGSG), the P2A self-cleaving peptide, and the 5′ 20 bases of the eGFP CDS to link together the Fezf1 CDS and eGFP in a HiFi reaction. The ultramer sequence was:

CGCGCCAAGCGCAGTGGGAGTGGTGGAAGCGGAGCTACTAACTTCAGCCTGCTGAAGCAGGCTGGAGACGTGGAGGAGAACCCTGGACCTATGGTGAGCAAGGGCGAGGA.

The *Fezf1* CDS was amplified using primers that created a 35 bp overlap between the CDS and the P2A ultramer; the P2A ultramer was amplified with complementary primers; and eGFP was amplified with primers specific to its CDS. These amplicons were then used in a HiFi reaction to generate the 3xHA-Fezf1-P2A-eGFP fragment. We then subcloned this fragment into pAAV-hSyn1-MCS to produce an AAV vector that allows for equimolar expression of 3xHA-Fezf1 and eGFP. The expression of pAAV-hSyn1-3xHA-Fezf1-P2A-eGFP was also validated in HEK293T cells.

shRNA Constructs

To make pAAV-hSyn1-DsRed-shRnd3, we modified the approach taken by (Peng et al., 2017) as follows. Short hairpin (sh) oligonucleotide was designed online (http://katahdin.mssm.edu/siRNA/RNAi.cgi?type=shRNA). The following sequences were used:

shRnd3

TGCTGTTGACAGTGAGCGAACAGGCAGACTCCTGTGTCATTAGTGAAGCCACAGATGTAATGACACAGGAGTCTGCCTGTGTGCCTACTGCCTCGGA

shScramble

TGCTGTTGACAGTGAGCGGCTGTTCCGCTCGTGTAGAGTTTAGTGAAGCCACAGATGTAAACTCTACACGAGCGGAACAGCTG
CCTACTGCCTCGGA

These oligos were separately amplified and cloned into pPRIME-DsRed-shCntn5 (Peng et al., 2017), replacing the shCntn5 sequence. DsRed expression was visualized in HEK293T cells for each construct. *shRnd3* knockdown efficacy was determined by western Blot as described previously (Wang et al., 2017) using lysates from HEK293T cells transfected with: 1) pCIG2-LSL-3xHA-Rnd3; 2) pCIG2-LSL-3xHA-Rnd3, pPRIME-DsRed-shRnd3, and pCAG-Cre; or 3) pCIG2-LSL-3xHA-Rnd3, pPRIME-DsRed-shScramble, and pCAG-Cre. Rabbit anti-HA (1:1000, Cell Signaling) and mouse anti-actin (1:20,000, Millipore) antibodies were used for western Blot. The DsRed-shRnd3 or DsRed-shScramble fragments were then subcloned into pAAV-hSyn1-MCS to generate final pAAV-hSyn1-DsRed-shRnd3 and pAAV-hSyn1-DsRed-shScramble constructs for producing adeno-associated viruses at the Janelia Research Campus Viral Tools Core.

In Utero Injection of AAVs

The procedure to introduce AAV in utero was similar to the targeted in utero electroporation surgery previously described (Hand et al., 2015). Timed pregnant E13.5 (shRNA experiments) and E14.5 (Fezf1 overexpression) CD1 females were deeply anesthetized with isoflurane and given buprenorphine at 0.1mg/kg body weight. The incision area was shaved, cleaned, and a small longitudinal incision was made to expose the embryos. The embryos were rinsed periodically with sterile dPBS. Sharp glass needles containing virus and fast green dye were pierced through the uterine wall, and into the eyes of targeted embryos. Virus was injected by mouth-pipette while slowly retracting the needle. One eye was injected per embryo, and around two-thirds of the embryos were injected per litter in order to prevent spontaneous abortion/pup loss. After injections, the embryos were gently placed back inside the abdominal wall and the incision was sutured and stapled. The dams were returned and recovered in a heated cage for several hours.

Tissue from embryonic and neonatal AAV transduction experiments were collected and processed at P14. Regions of interest for imaging and quantification were selected based on high viral transduction, defined by transduced horizontal cells in the outer retina overlying a given region of interest.

QUANTIFICATION AND STATISTICAL ANALYSIS

Analysis of mosaic spacing was conducted as previously described (Kay et al., 2012; Peng et al., 2017). Briefly, cell number from a 212.55 X 215.55 μm square region was counted at 8-10 locations per retina (2 retinas per genotype). X-Y cell coordinates marked manually were used to calculate DRP statistics. The distance of exclusion zone radius, packing factor and nearest-neighbor regularity indexing (data to random) were then calculated using WinDRP software.

To define the prominent process, processes from a cell were traced and measured using simple neurite tracing (ImageJ). The longest process, longer than 20 μm, was defined as a prominent process. The angle ROI function (ImageJ) was then used to measure the angle of the prominent process with 0° corresponding to a line perpendicular to the apical surface of the retina. A polar plot of showing lengths and angles was generated using SigmaPlot (Sigma) software.

All data are shown as Mean ± SEM with n representing the sample number from at least two mice or independent experimental replicates. Two-tailed Student's t tests were used for two group comparisons. One-way ANOVA with post hoc Tukey HSD was used for multi-group comparisons. Statistical details can be found in Figures and Figure Legends.

DATA AND CODE AVAILABILITY

The accession number for the raw and processed scRNA-seq and RNA-seq data reported in this paper is GEO: GSE132555.